Cloud condensation nuclei in pristine tropical rainforest air of Amazonia: size-resolved measurements and modeling of atmospheric aerosol composition and CCN activity

S. S. Gunthe[1], S. M. King[2], D. Rose[1], Q. Chen[2], P. Roldin[3], D. K. Farmer[4], J. L. Jimenez[4], P. Artaxo[5], M. O. Andreae[1], S. T. Martin[2], and U. Pöschl[1]

(1) Max Planck Institute for Chemistry, Biogeochemistry Department, Mainz, Germany

(2) Harvard University, School of Engineering and Applied Sciences & Department of Earth and Planetary Sciences, Cambridge, MA, USA

(3) Lund University, Nuclear Physics, Faculty of Technology, Lund, Sweden

(4) University of Colorado, Dept. of Chemistry & Biochemistry and CIRES, Boulder, CO, USA

(5) Instituto de Fisica, Universidade de Sao Paulo, Sao Paulo, Brazil

Correspondence to: S. Gunthe (gunthe@mpch-mainz.mpg.de)

Supplementary Material for the Discussion Paper to be published in ACPD

Version/Date: 18 December 2008

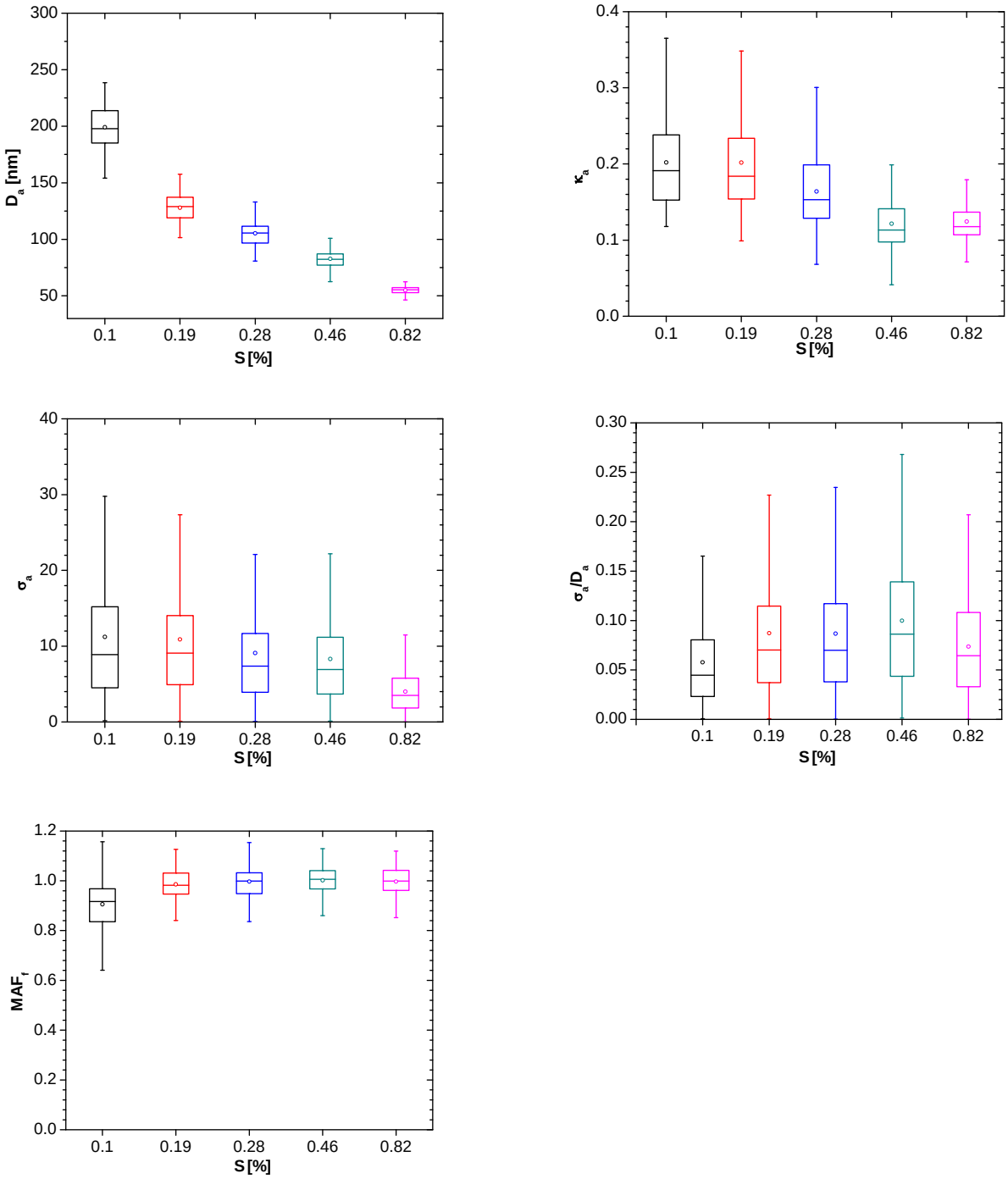

Fig. S1: Statistical distribution of characteristic parameters derived from the CCN efficiency spectra (3-parameter CDF fits) observed at different supersaturations for the entire campaign. Box with bars indicates 5th, 25th, 50th, 75th, and 95th percentile and dot indicates the arithmetic mean value.

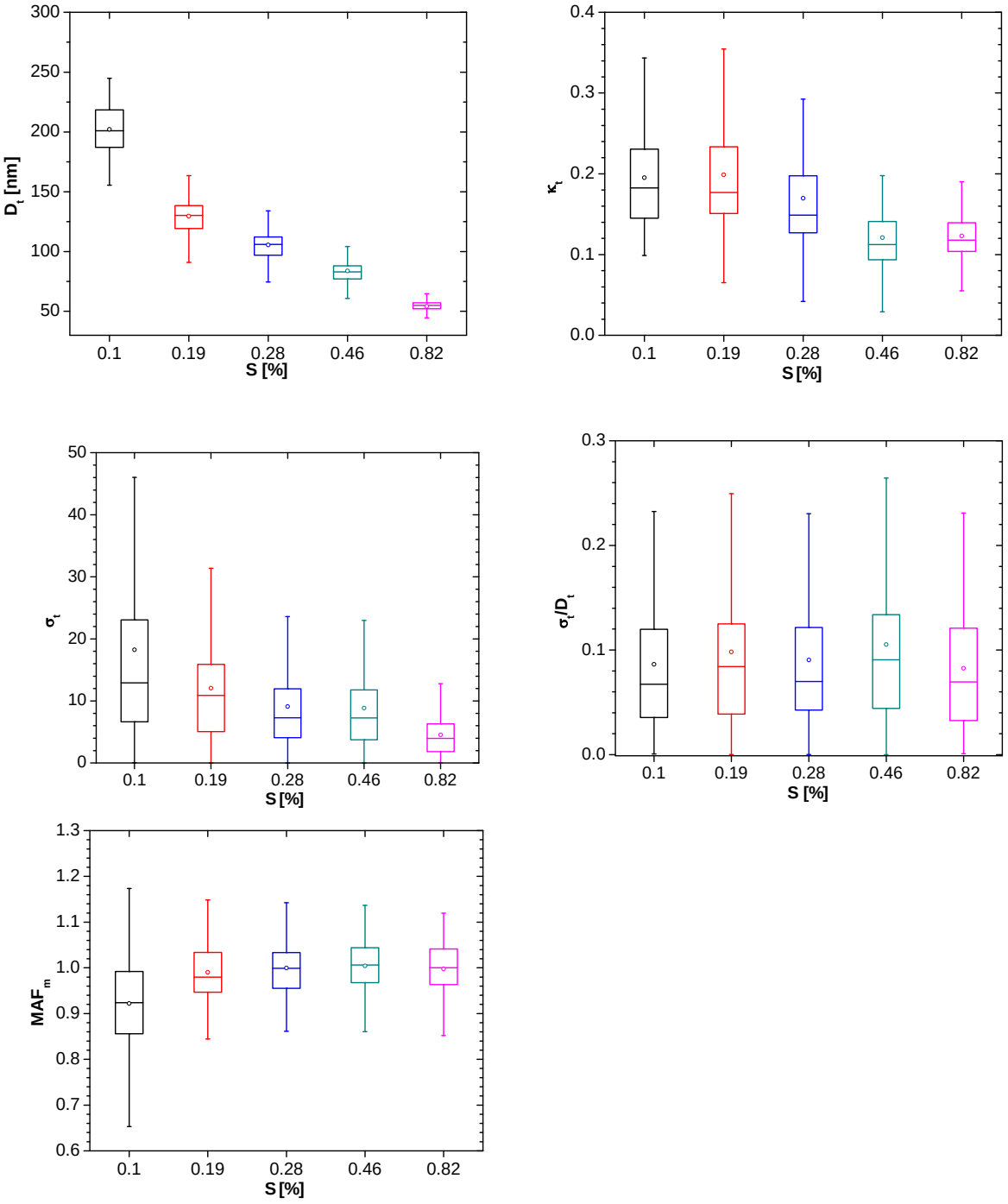

Fig. S2: Statistical distribution of characteristic parameters derived from the CCN efficiency spectra (2-parameter CDF fits) observed at different supersaturations for the entire campaign. Box with bars indicates 5th, 25th, 50th, 75th, and 95th percentile and dot indicates the arithmetic mean value.

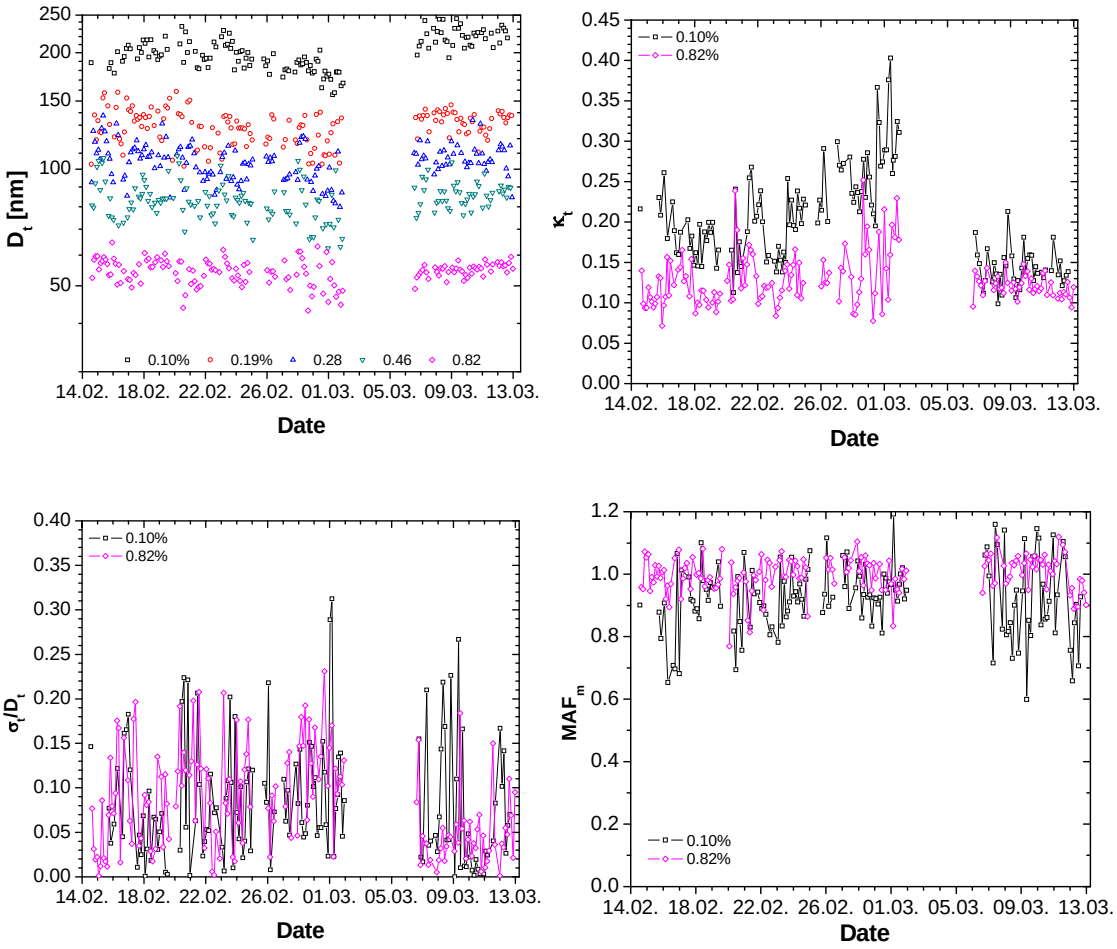

Fig. S3: Time series of characteristic parameters derived from the CCN efficiency spectra (2-parameter CDF fits) observed at different supersaturation levels (S=0.10-0.82%) plotted against the date in Feb-Mar 2008 (UTC): midpoint activation diameter (D_t), effective hygroscopicity diameter (κ_t), heterogeneity parameter (σ_t / D_t), and measured maximum activated fraction (MAF_m).

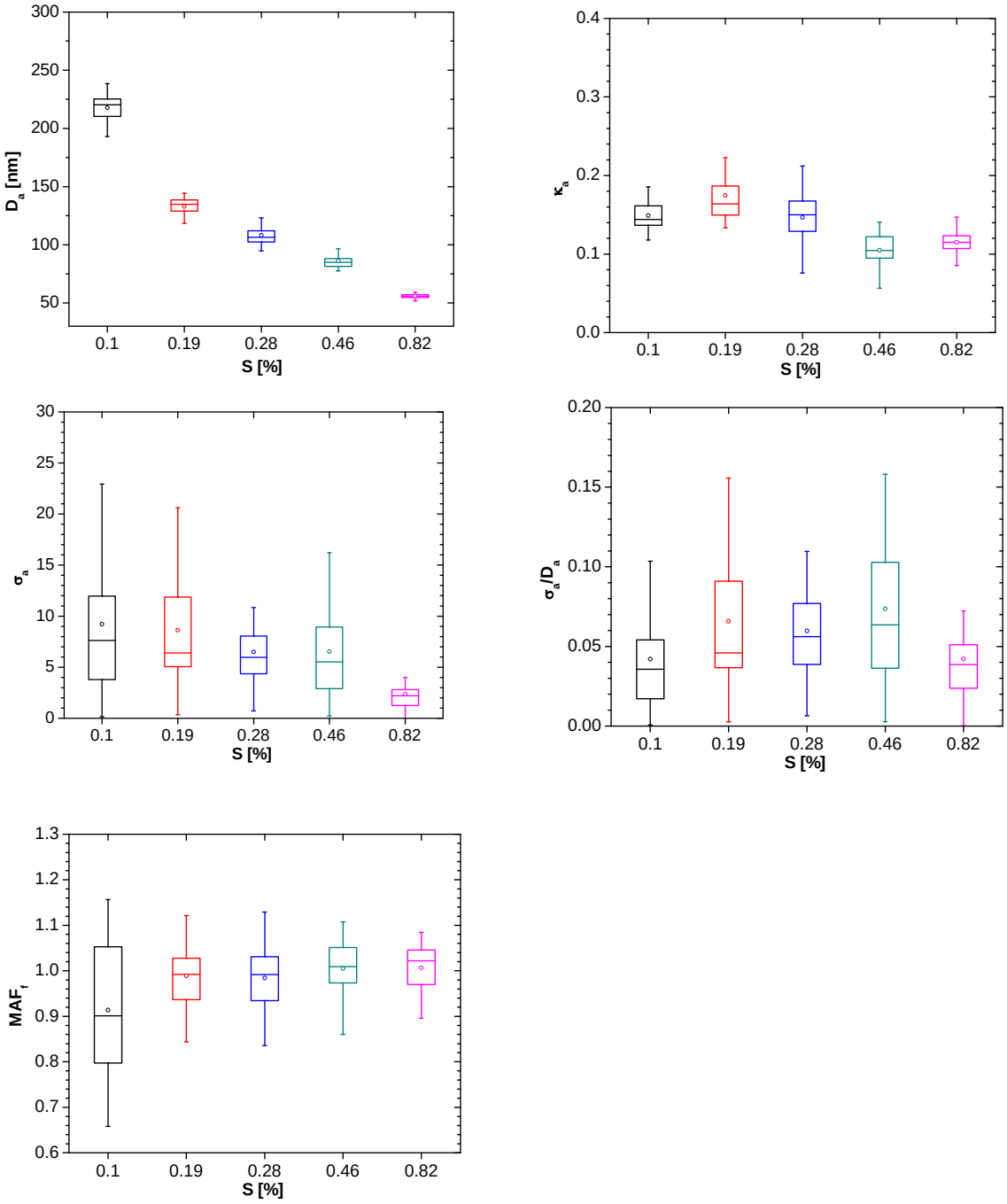

Fig. S4: Statistical distribution of characteristic parameters derived from the CCN efficiency spectra (3-parameter CDF fits) observed at different supersaturations during the focus period, 6-12 March 2008. Box with bars indicates 5th, 25th, 50th, 75th, and 95th percentile and dot indicates the arithmetic mean value.

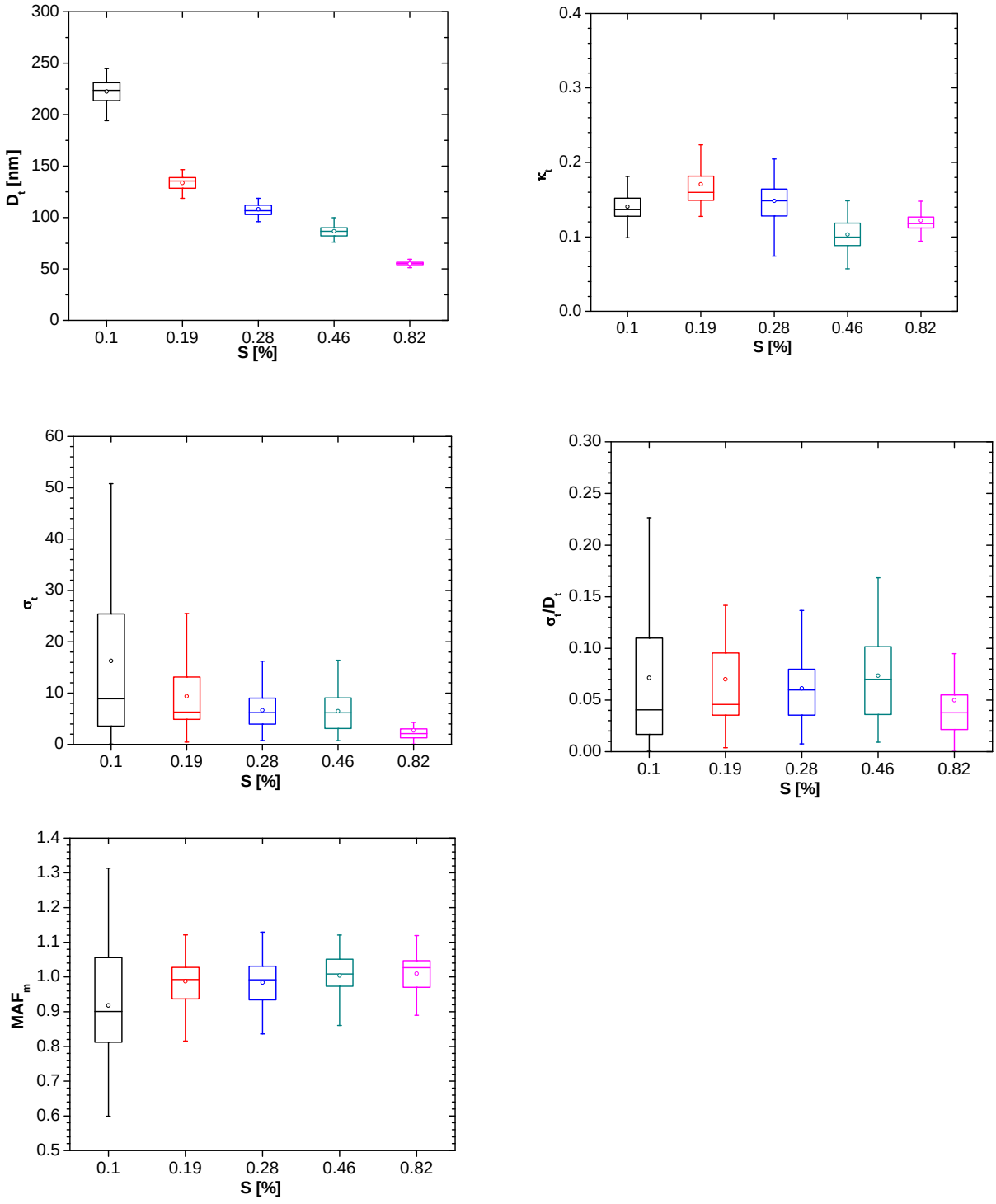

Fig. S5: Statistical distribution of characteristic parameters derived from the CCN efficiency spectra (2-parameter CDF fits) observed at different supersaturation levels during the focus period, 6-12 March 2008. Box with bars indicates 5th, 25th, 50th, 75th, and 95th percentile and dot indicates the arithmetic mean value.

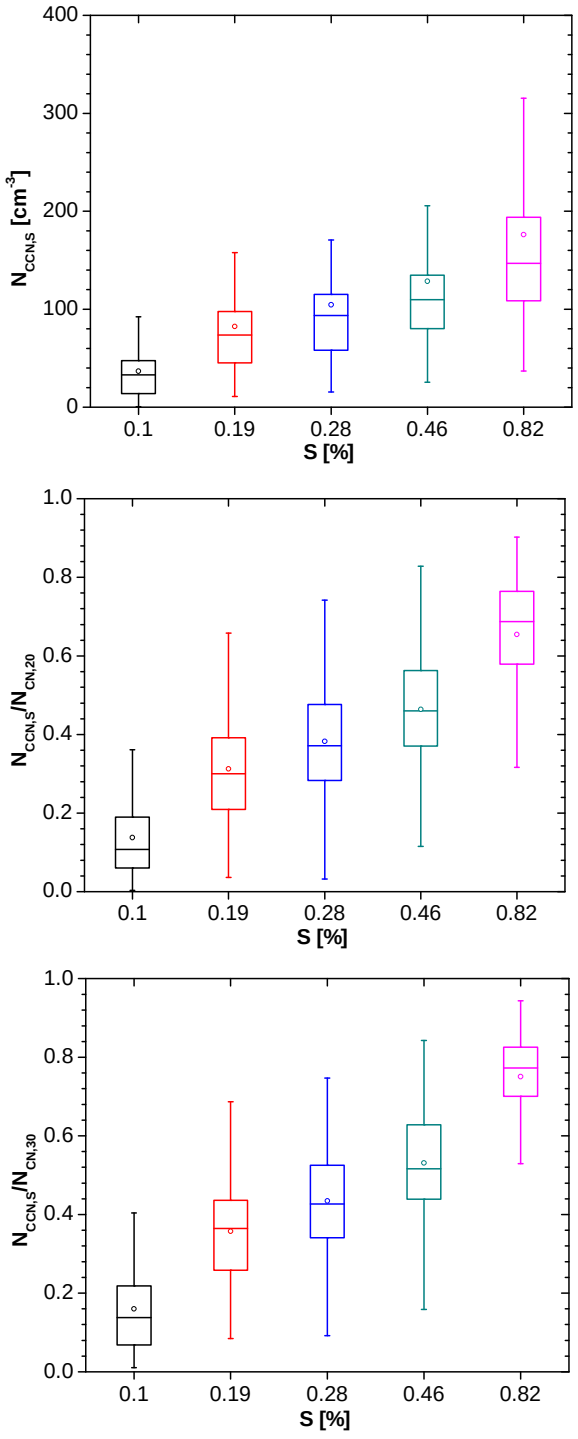

Fig. S6: Statistical distribution of CCN number concentrations ($N_{CCN,S}$) and integral CCN efficiencies ($N_{CCN,S}/N_{CCN,20}$, $N_{CCN,S}/N_{CCN,30}$) observed at different supersaturations for the entire campaign. Box with bars indicates 5th, 25th, 50th, 75th, and 95th percentile and dot indicates the arithmetic mean value.

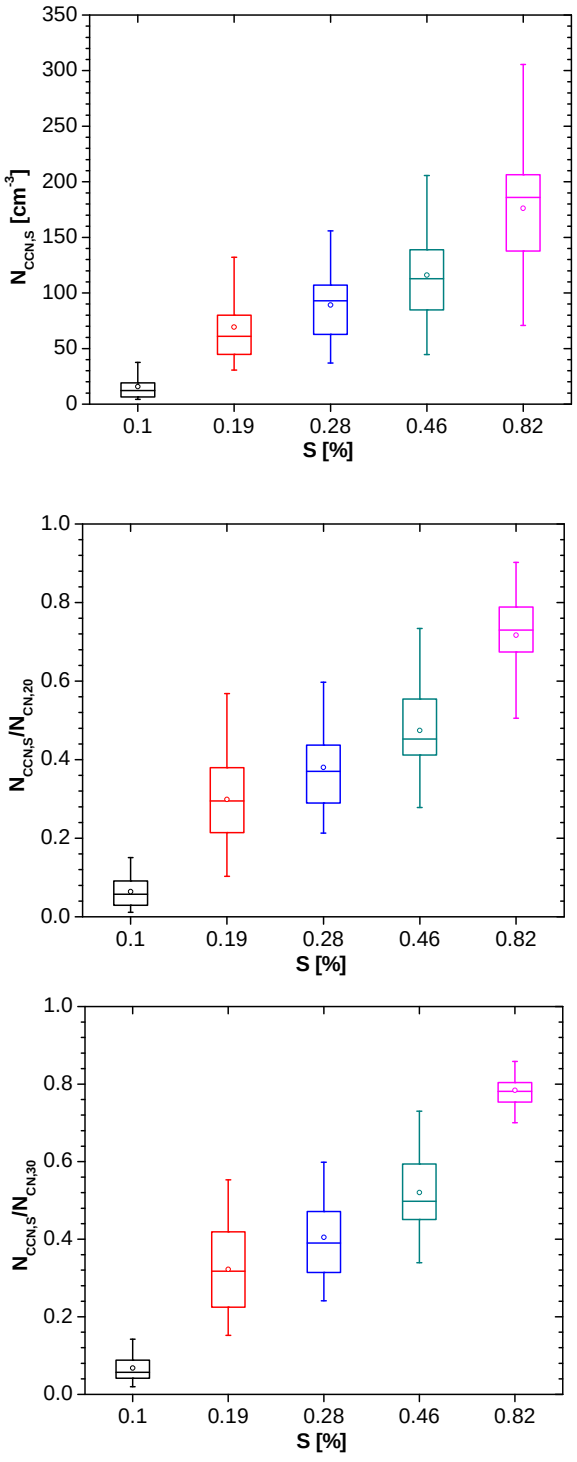

Fig. S7: Statistical distribution of CCN number concentrations ($N_{CCN,S}$) and integral CCN efficiencies ($N_{CCN,S}/N_{CCN,20}$, $N_{CCN,S}/N_{CCN,30}$) observed at different supersaturations during the focus period, 6-12 March 2008. Box with bars indicates 5th, 25th, 50th, 75th, and 95th percentile and dot indicates the arithmetic mean value.

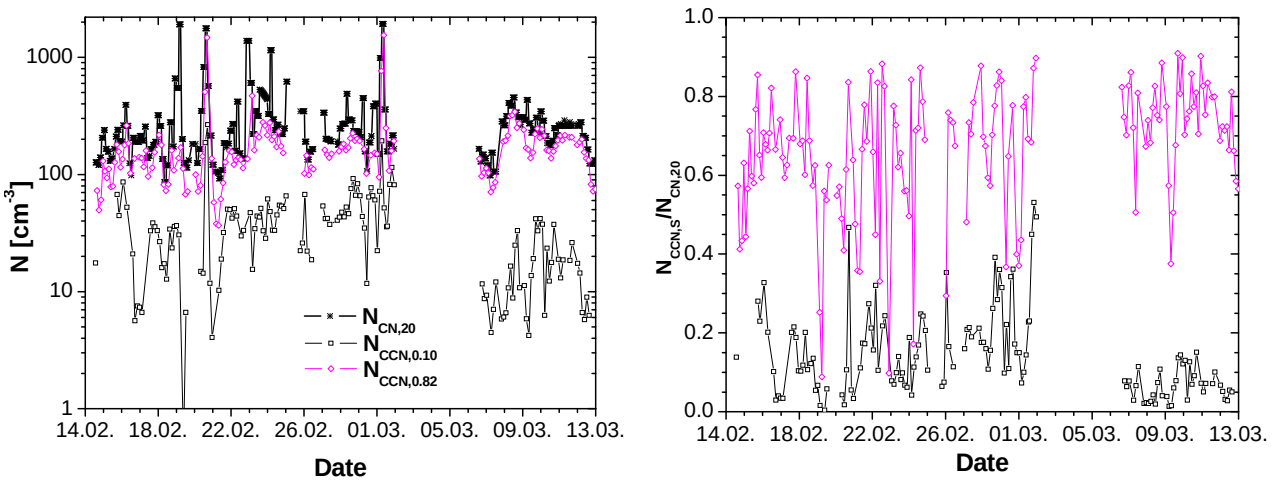

Fig. S8: Time series of (a) the number concentrations of total aerosol particles ($N_{CN,20}$) and cloud condensation nuclei ($N_{CCN,S}$), (b) the integral CCN efficiencies ($N_{CCN,S}$/ $N_{CN,20}$) at different supersaturation levels (S=0.10% and 0.82%) plotted against the date in Feb-Mar 2008 (UTC).

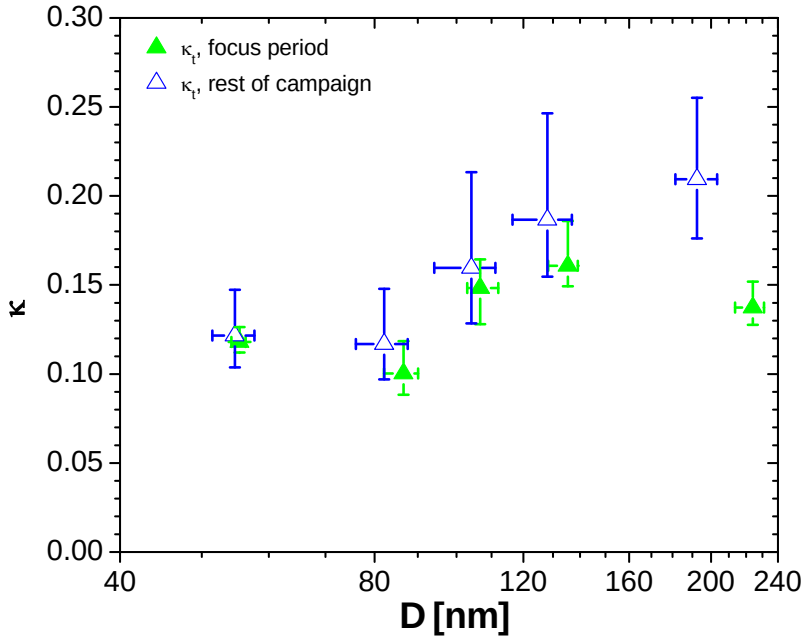

Fig. S9: Effective hygroscopicity parameters averaged over the focus period and over the rest of the campaign (κ_t as derived from 2-parameter CDF fits to the measured CCN efficiency spectra). The data points are median values corresponding to a given level of supersaturation, and the error bars extend to upper and lower quartiles.

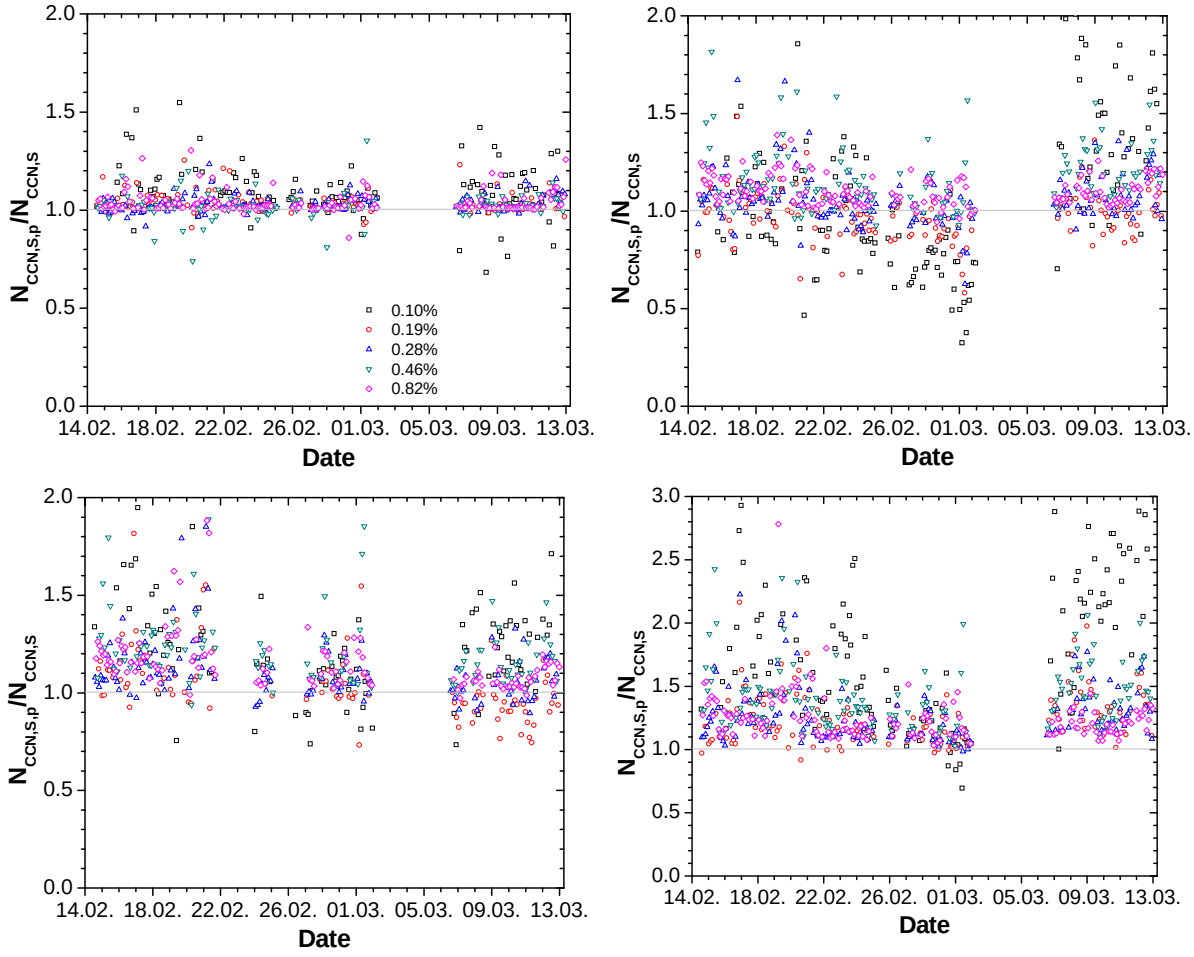

Fig. S10: Time series of the ratio of predicted and measured CCN concentrations ($N_{CCN,S,p}/N_{CCN,S}$) plotted against the date in Feb-Mar 2008 (UTC). Predictions are based on the κ-Köhler model approach using different types of effective hygroscopicity parameters: (a) with variable values of κ_t as derived from the individual CCN efficiency spectra; (b) with a constant average value of $\kappa_t = 0.159$; (c) with variable values of κ_p predicted from the organic and sulfate mass fractions determined by AMS; and (d) with a constant global average value of κ=0.3.

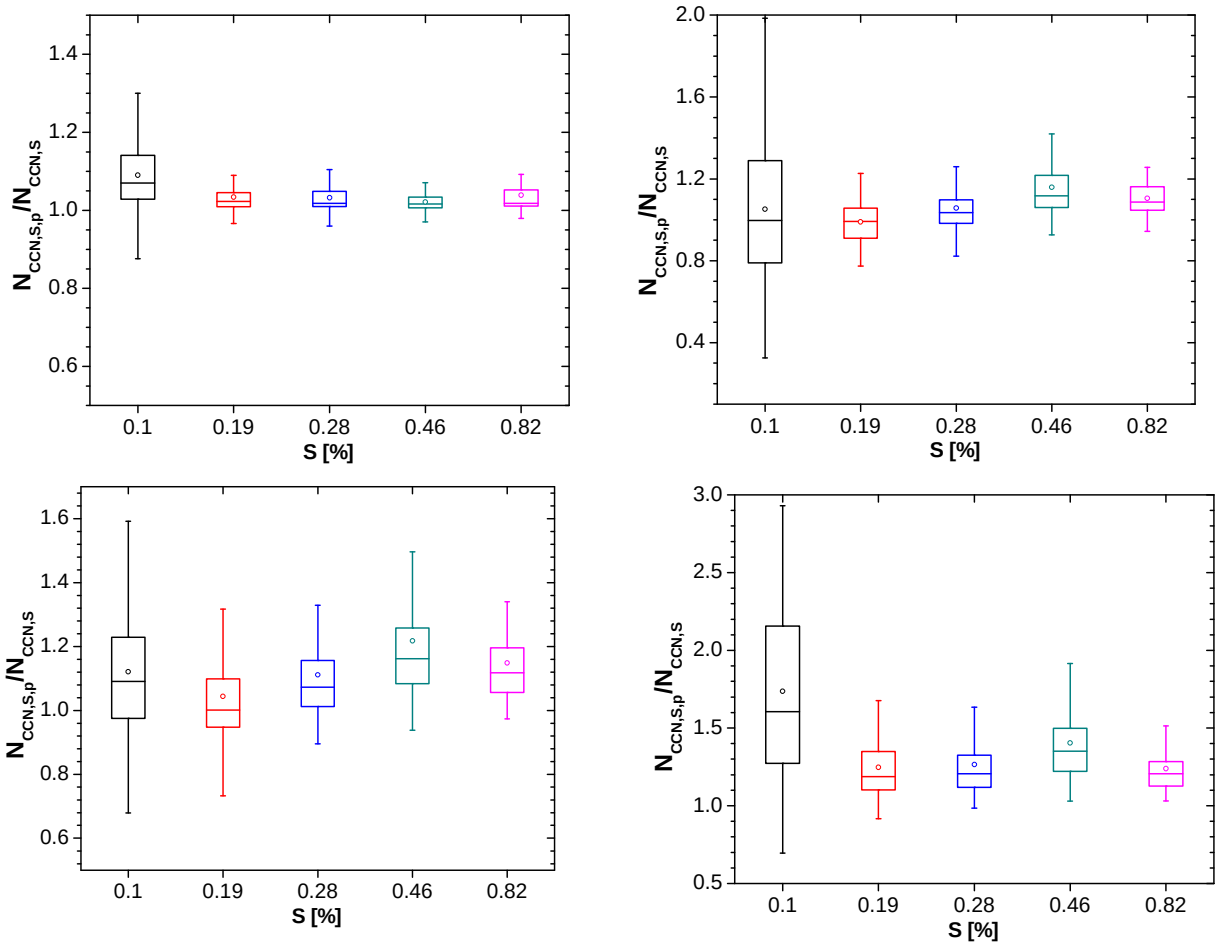

Fig. S11: Statistical distribution of the ratios of predicted and measured CCN concentrations ($N_{CCN,S,p}/N_{CCN,S}$) at different supersaturation level over the entire campaign. Predictions are based on the κ-Köhler model approach using different types of effective hygroscopicity parameters: (a) with variable values of κ_t as derived from the individual CCN efficiency spectra; (b) with a constant average value of $\kappa_t = 0.147$; (c) with variable values of κ_p predicted from the organic and sulfate mass fractions determined by AMS; and (d) with a constant global average value of κ=0.3. Box with bars indicates 5th, 25th, 50th, 75th, and 95th percentile and dot indicates the arithmetic mean value.

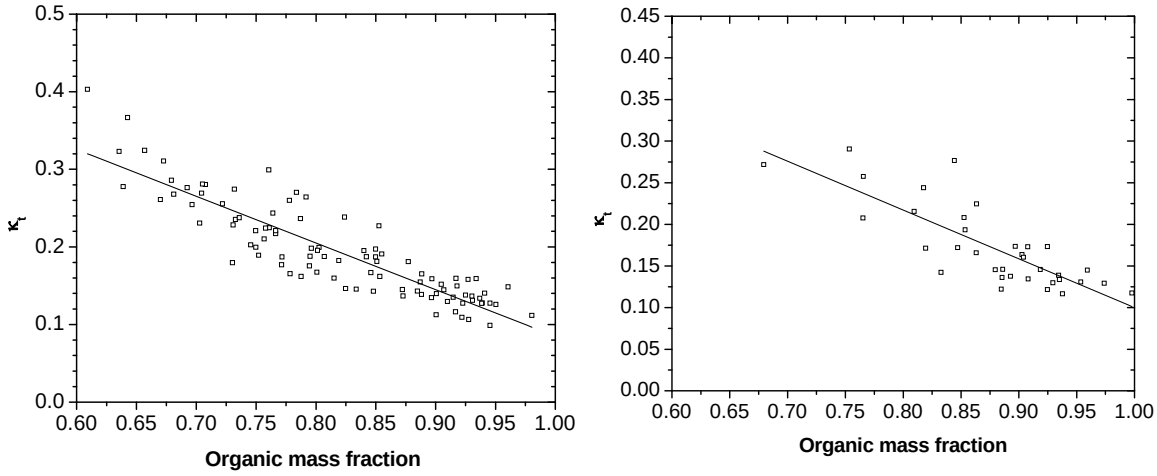

Fig. S12: Correlations between the effective hygroscopicity of CCN (κ_t) observed at S = 0.1% and the organic mass fraction ($X_{m,org}$) determined by (a) integral and (b) size-resolved AMS measurements. Linear fit equations, correlation coefficients, and numbers of data points: (a) y=0.696-0.600x, R^2=0.79, n=97; (b) y=0.686-0.587x, R^2=0.65, n=36